Spin Determination of Intermediate Structure in the Subthreshold Fission of ^{237}Np†

G. A. Keyworth, J. R. Lemley,* C. E. Olsen, and F. T. Seibel
Los Alamos Scientific Laboratory, University of California, Los Alamos, New Mexico 87544

J. W. T. Dabbs and N. W. Hill
Oak Ridge National Laboratory, Oak Ridge, Tennessee 37830
(Received 20 July 1973)

A polarized neutron beam and a polarized target have been used to determine spins of 15 intermediate structure groups observed in the fission of ^{237}Np below 1 keV and of 94 resonances observed in transmission below 102 eV. The pulsed neutron beam, from the Oak Ridge electron linear accelerator, was polarized by transmission through a dynamically polarized proton sample. The ^{237}Np, in the ferromagnetic compound $NpAl_2$, was cooled by a ^{3}He-^{4}He dilution refrigerator. Nine individual fine-structure resonances comprising the first group at 40 eV were determined to have the same spin, $J=3$, substantiating the current interpretation of intermediate structure in subthreshold fission in terms of the Strutinsky double-humped deformation barrier. Correlation of these results with existing data on the angular distribution of fission fragments from aligned ^{237}Np indicates an apparent admixing of transition states, as evidenced by nonintegral values of the projection quantum number, K.

[NUCLEAR REACTIONS, FISSION ^{237}Np(n,f), $E=1$, 1000 eV; measured $\sigma(E)$, J; ^{237}Np+n total σ; $E=1$–102 eV; measured $\sigma(E)$, J; polarized neutrons, polarized target.]

I. INTRODUCTION

In 1966, Strutinsky[1] introduced a theory of nuclear energies as a sum of a liquid-drop term and a correction due to shell effects which explained the presence of spontaneously fissioning isomers. For actinide elements, this theory predicts a secondary minimum in the curve relating potential energy to the deformation. Since 1967, substantial evidence of intermediate structure in the subthreshold fission cross sections of nuclides in the mass range 230–252 has become available. Lynn[2] and Weigmann[3] ascribed the observed intermediate structure to coupling of the compound nuclear or "class I" states corresponding to the ground-state deformation of the nucleus and "class II" states in the second minimum corresponding to large deformation. Consequently, the individual fission resonances comprising the observed structure should have the same spin and parity as the "class II" state.

The observation of narrow intermediate structure in the fission cross section of ^{237}Np was first reported by Paya *et al.*[4,5] Although the total cross section is undistinguished, with a level spacing for both s-wave neutron-induced spin states of 0.67 eV, the fission cross section is composed of numerous structures whose mean level spacing is ~60 eV. The fission widths of the larger individual resonances comprising these structures are as much as 1000 times greater than the fission widths of the background resonances.

Attempts to determine spins of compound nuclear states in fissioning nuclei have primarily been made by indirect methods, such as by observing high-energy capture γ rays deexciting the compound nuclear states, relative γ-ray multiplicities, combination of partial and total cross sections, and measuring the ratio of symmetric to asymmetric fission. The direct method utilizing a polarized neutron beam and polarized fissionable targets has previously been limited to neutron energies below 10 eV. Because of these limitations and because of the inconsistencies in those spin assignments which do exist for fissionable nuclei, an experimental program to utilize polarized targets and a polarized neutron beam of uniform polarization over the energy range 1 to 50 000 eV with time-of-flight techniques has been undertaken. In this report, spin assignments of the prominent structures in the fission cross section over the incident neutron energy range 1 to 1000 eV are made and of resonances in the total cross section from 1 to 102 eV.

Because this is the first experiment reported in this program and because these same techniques have not previously been used in a single experiment, the experimental methods are described in some detail. The theoretical background and methods of data reduction are discussed briefly

and the results are interpreted in terms of the double-humped fission barrier as well as spin-dependent statistical properties of nuclei.

II. EXPERIMENTAL METHOD

The apparatus used in these measurements consists of a dynamically polarized sample of protons in single crystals of $La_2Mg_3(NO_3)_{12}24H_2O$, hereafter abbreviated LMN, a ^{3}He-^{4}He dilution refrigerator and superconducting coil to polarize a target of ^{237}Np, and an array of neutron detectors to measure both fission neutrons and the transmitted beam.

A. Polarization of the Neutron Beam

Stolovy[6] and Postma *et al.*[7] have demonstrated the technique of polarizing neutrons by Bragg reflection from a magnetized cobalt-iron crystal to obtain high polarization for neutrons from thermal energy to approximately 10 eV. Similarly, nuclear reactions, such as ^{7}Li(p,n), are effective at energies above 100 keV. However, in the range 10 eV to 100 keV, these techniques lead to rather low neutron polarizations.

In 1966 Shapiro[8] reported the use of a dynamically polarized proton sample to obtain a polarized beam of neutrons. Using this method of neutron polarization and a polarized target of ^{165}Ho, the spins of a number of neutron resonances in holmium were determined. This method utilizes the strong spin dependence of the neutron-proton interaction where the cross section for scattering through the singlet state of the system is approximately 20 times larger than that for scattering through the triplet state. Thus, an unpolarized neutron beam becomes polarized when filtered through a polarized proton sample. Since the cross sections of singlet and triplet scattering vary little over the energy range 1 eV–50 keV, the polarization of the transmitted beam is essentially constant over this range.

The method of dynamic nuclear polarization of protons in LMN owes its success to the pioneering achievements of Jeffries[9] and of Abragam and Borghini.[10] If one considers a magnetically dilute solid containing free electron spins and proton spins in simple dipolar coupling, the energy levels are given by

$$E(M,m) \approx g\beta MH - g_p\beta mH\,, \qquad (1)$$

where M and m are the magnetic quantum numbers of the free electron and proton, respectively. The energy levels are shown in Fig. 1, where $\nu_e = g\beta MH/h$ and $\nu_p = g_p\beta mH/h$, the electron and proton magnetic resonance frequencies, and τ_i are the spin-lattice relaxation times for the various transitions. If τ_1, the electron relaxation time is small compared to $\tau_2 = \tau_3$, the proton-electron relaxation time, then application of radiation of frequency $\nu_e \pm \nu_p$ will result in a net bulk polarization of the protons. Very simply, a flip-flip ($\Delta M = 1$, $\Delta m = 1$) transition is induced and the electron relaxes to induce another flip-flip transition while the proton remains in its "flipped" state because of its longer relaxation time. Because the free-electron system is initially polarized, at a low temperature and in an applied magnetic field H, then the proton system will be polarized, after microwave pumping. LMN is such a system, where the free electrons are paramagnetic ions of $^{142}Nd^{3+}$, replacing ~1% of the La^{3+} ions, and the free protons are in the water of hydration.

The major practical difficulty in using LMN is that the pumped transition is forbidden and, hence, the line width is narrow, $\Delta\nu/\nu \sim 0.03\%$, requiring a stable and uniform magnetic field over the entire crystal volume and a stable source of microwave radiation to achieve high bulk polarization.

The cryogenic system used in this experiment is shown in Fig. 2. The cryostat contains two liquid helium baths; the inner, operating at a temperature of ~1.15°K, contains the LMN crystals and a superconducting split coil, while the

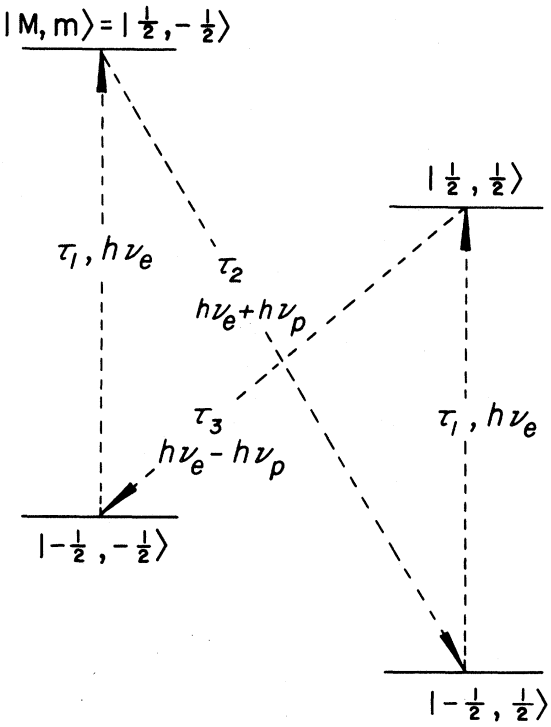

FIG. 1. Energy levels and transitions for a proton in dipole-dipole coupling with an electron.

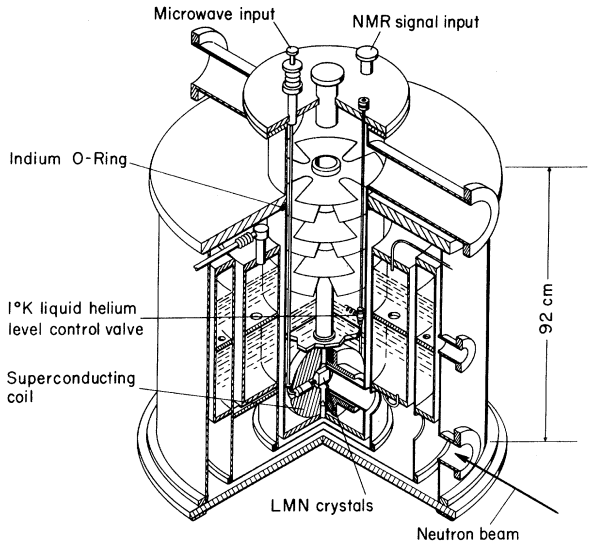

FIG. 2. Cryostat containing the dynamically pumped polarized proton sample.

annular vessel contains liquid helium at atmospheric pressure. The two liquid helium containers are connected through a thin stainless steel tube with a needle valve to compensate for the helium which boils away in the inner vessel. The level of 1.15°K helium may be maintained constant provided some helium remains in the outer bath. The outer bath is surrounded by another annular vessel containing liquid nitrogen serving as a shield against ambient thermal radiation. The inner vessel and sections of the helium and nitrogen transfer lines are fabricated of stainless steel, while the remainder of the cryostat is aluminum. Joints between stainless steel and aluminum are soldered except where demountable seals are required. The entire cryogenic system may be readily disassembled, although its considerable size (104-cm diam × 128-cm height) makes this operation somewhat awkward. In transit, the neutron beam passes through two 0.13-mm and two 0.25-mm stainless steel foils, and two 0.13-mm copper windows in the cylindrical microwave cavity, in addition to the LMN crystals. The vacuum pump required to maintain the inner liquid helium bath at 1.15°K is a Rootes-type blower of 1400-liters-per-second capacity. The liquid helium consumption rate of the cryogenic system is about 200 liters per day.

The magnetic field is generated by a superconducting split-coil wound of NbTi monofilament. Its design includes correction to eighth order and the errors introduced in winding and by nonuniform wire are compensated by trim coils. The homogeneity of the magnetic field over the 18-cm^3 crystal volume was measured to one part in 10^5 at the design field of 20.3 kOe. The power supply used to energize the coil is a highly current-regulated 75-A unit, manufactured by Intermagnetics General Corporation. After energizing, the magnet was operated in the persistent mode and no decay in the magnetic field was observed during periods of 36 hours.

The microwave source used is an extended interaction oscillator manufactured by Varian Associates of Canada. Its maximum power output at 77 GHz is about 10 W. This oscillator is quite stable, when used with a well-regulated power supply and cooled with temperature-controlled water, as evidenced by the fact that no observable change in polarization normally occurred during 24-h runs. The oscillator may be electronically tuned ±125 MHz or mechanically tuned ±1 GHz. Partially due to a frequency dependence in the output power and partially to the difficulty in measuring the frequency with the required precision, the proton polarization was reversed by adjusting the current through the magnet, rather than by changing the microwave frequency.

The polarization was measured by both NMR techniques and by measuring the transmission of neutrons. In the former case, a single turn coil was wrapped on each end of a hydrogen-free fluorocarbon form which holds the LMN crystals. A small fraction of the protons in the target were caused to flip by an rf field at the proton magnetic resonance frequency (~87 MHz at 20.3 kOe). The coil is tuned to the same frequency by a voltage variable capacitor. The polarization is then determined from measurement of the absorption of energy from the tuned circuit when the protons are positively polarized, and a net transfer of energy to the circuit for negative polarization. The difficulty with this method is that the amplitude of the signal at thermal equilibrium, corresponding to a polarization ~0.2%, must be accurately determined and compared to the signal after microwave pumping to determine the absolute polarization. The NMR system used in this experiment utilized the fast-sweep technique, in which the frequency of the oscillator is swept sufficiently rapidly to permit a continuous display of the proton line on an oscilloscope. However, in order to see the thermal equilibrium signal, signal averaging was required.

The dependence of the transmission of the incident unpolarized neutrons upon the proton polarization is given by the expression[8]

$$T = \exp(-X)\cosh\frac{\Sigma_p}{\Sigma} f_N X, \tag{2}$$

where

$$f_n = \tanh\frac{\Sigma_p}{\Sigma} f_N X . \quad (3)$$

The total macroscopic cross section, Σ, has been determined for LMN by Draghicescu *et al.*,[11] as has the macroscopic polarization cross section, Σ_p. In these expressions, $X=\Sigma t$ is the target thickness in units of the neutron mean free path in the target, while f_N and f_n are the polarization of the protons and of the transmitted neutrons, respectively. In Fig. 3, the dependence of T and f_n upon the proton polarization, f_N, is presented. Clearly, an accurate measurement of the transmission permits precise determination of the average proton polarization. In addition to greater precision, an advantage of this method over NMR techniques is that it averages over the entire volume of LMN. This fact was demonstrated by the observation that the maxima in transmission and in NMR signal occur at slightly different microwave frequencies, indicating a shift in magnetic field from the bulk of the crystal volume to the volume sampled by the NMR coils. The transmission was measured with a 0.5-mm-thick lithium-glass scintillator (NE912) enriched in ^{6}Li, manufactured by Nuclear Enterprises, Inc. The measurement permitted to deduce the polarization of the transmitted neutrons with an estimated accuracy of ±2%. The operating parameters of the LMN system are given in Table I.

B. Polarization of the Target

In contrast to the dynamic polarization method discussed above, thermal equilibrium techniques are most applicable in polarizing fissionable nuclei. The simplest of the thermal equilibrium methods is the brute-force method, whereby the interaction between an externally applied magnetic field with the nuclear magnetic moment at low temperatures results in a polarization given by

$$f_N \approx \frac{1}{3}\,\frac{I+1}{I}\,\frac{\mu H}{kT} . \quad (4)$$

This method offers the advantage that any nucleus with intrinsic spin and with a magnetic moment may be polarized. However, for any appreciable polarization, the necessary combination of magnetic field and temperature is extremely difficult to achieve (e.g., a magnetic field of 50 kOe and temperature of 0.1°K result in a polarization of 2.4% for ^{237}Np).

Currently, the most widely used method of achieving nuclear polarization is the use of magnetic hyperfine splitting in paramagnetic or ferromagnetic systems. The disadvantage of using paramagnetic salts (the method of Gorter[12] and Rose[13]) is that the salts are generally dilute in the desired nucleus and they normally have extremely poor thermal conductivity. The low conductivity almost precludes using this method with radioactive nuclei. Both these problems are overcome by using a ferromagnetic metallic compound. In ferromagnets the alignment of electronic spins produces large internal magnetic fields with resultant high nuclear polarization. The difficulty in selecting a suitable material for polarizing actinide nuclei is that the systematics of magnetic behavior of actinide compounds are complex and poorly known. The hyperfine fields in a large number of compounds have been determined, primarily using the Mössbauer effect, but the magnetic behavior at low temperatures is not known. In particular, it is generally uncertain as to whether a compound is ferromagnetic or antiferromagnetic.

In this particular experiment, the intermetallic compound $NpAl_2$ was selected as the target material. This compound is known[14] to have a saturation hyperfine field of 3.155 MOe and a Curie temperature of 56°K. These facts, combined with its metallic nature, implying relatively good thermal conductivity, make the dialuminide appear to be an ideal sample material. In addition, sample

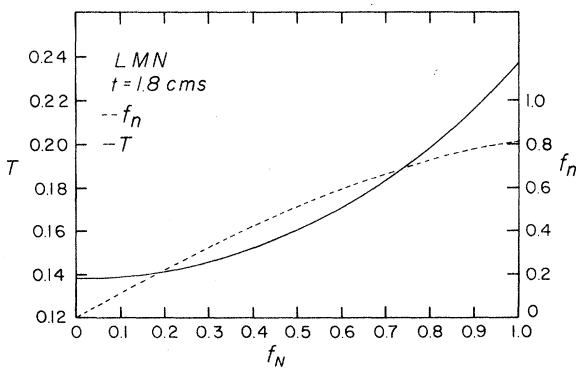

FIG. 3. The transmission of the neutron beam and the neutron polarization vs proton polarization for a 1.8-cm-thick LMN sample.

TABLE I. LMN operating parameters.

Target volume	18 cm^3
Magnetic field	20.3 kOe
Microwave frequency	$\nu_e \pm \nu_p = 76.7 \pm 0.086$ GHz
Microwave power	~1 W
Liquid helium consumption	~200 liters/day
Pumping speed	1400 liters/sec
Ratio Nd/La	1%
Proton relaxation time	60 min
Average proton polarization	55%

preparation was reasonably straightforward.

The Np metal, received in the form of a reduced button, was broken into several pieces which were cleansed of adhering oxide and slag by electropolishing the metal (as the anode) in a solution of 25 g of potassium carbonate dissolved in 100 ml of distilled water. A piece of the neptunium metal weighing approximately 3 g was melted with a stoichiometric amount of high-purity aluminum in an inert-atmosphere arc melter. The argon atmosphere was first cleansed by melting a zirconium getter button. The sample was rotated and frequently remelted. The $NpAl_2$ button, which appears to be stable in air, was crushed in an inert-atmosphere glove box and mixed with aluminum powder so that the volume of aluminum was three times that of the $NpAl_2$. This mixture was tumbled and then pressed into the sample holder at a pressure of 3400 atm, resulting in a cold-sintered metallic-appearing sample.

The heart of the cryogenic system is a ^{3}He-^{4}He dilution refrigerator, designed and fabricated by the S. H. E. Manufacturing Corp.[15] A dilution refrigerator utilizes the fact that the dissolving of ^{3}He in ^{4}He is a heat-absorbing process, to produce sustained temperatures from 0.3 to below 0.01°K. This process offers numerous advantages over the adiabatic demagnetization method. Of principal pertinence to this experiment is that the continuous cooling power of a dilution refrigerator permits operating with radioactive elements at a constant temperature for nearly unlimited periods of time whereas the natural heating from the radioactive decay would imply a rapidly rising sample temperature in a demagnetized salt of any practical size. This particular dilution refrigerator was designed with the primary intent of attaining minimum temperatures, resulting in some loss in maximum cooling power. The minimum temperature attained was 8 mK, measured 15 cm from the mixing chamber (where the actual cooling takes place) on a copper rod. This temperature was determined by measuring the anisotropy of γ rays from a sample of ^{54}Mn in iron[16]

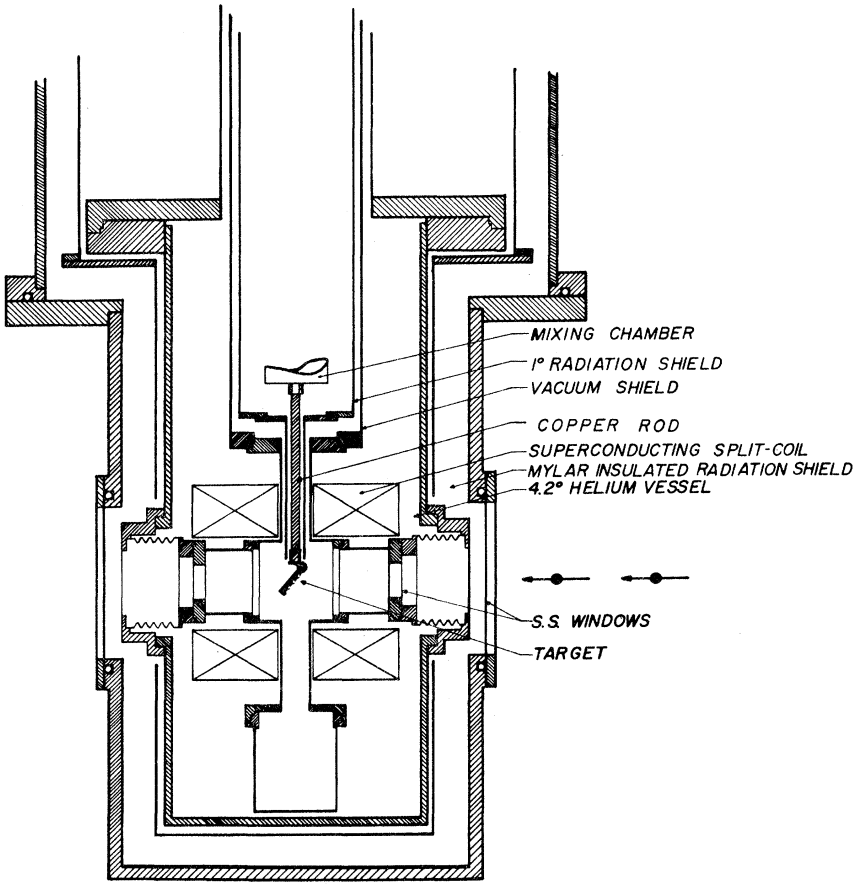

FIG. 4. The lower portion of the ^{3}He-^{4}He dilution refrigerator cryostat.

and represents the minimum reproducible temperature with no heat load. With a heat load of 500 ergs/sec, equivalent to 2.5-g ^{237}Np, a temperature of 135 mK at the outside of the mixing chamber was realized.

The lower portion of the cryostat is shown in Fig. 4. Space limitations at the Oak Ridge electron linear accelerator (ORELA) required that the targets be accessible through the bottom of the cryostat without removal of the refrigerator. Thus a number of indium O-ring seals were used to permit disassembly of that portion of the cryostat which surrounds the target. All components except the outer room-temperature container are fabricated of stainless steel. The incident polarized neutron beam passes through two stainless steel foils of total thickness 0.1 mm before striking the target. The system uses 25 liters/day of liquid helium.

The target is surrounded by a superconducting split-coil fabricated by American Magnetics, Inc. The coil is unusual in that the two coils may be separated to a distance of 25 cm. In operation the two coils were maintained 2 cm apart by a spacer of high-strength type-7075 alloy aluminum. This material was selected to allow minimum attenuation of the neutrons emitted in fission. The superconducting element is multifilament NbTi wire and is wound on a stainless steel form. The coil is capable of producing a maximum field of 55 kOe at an energizing current of 65 A.

The normal operating field of the coil was 15 kOe. Initially, the field was raised to 45 kOe and maintained while the sample was cooled through the Curie temperature to a temperature below 1°K. The field was then reduced to 15 kOe and put in the persistent mode. Cooling through the ferromagnetic transition temperature in an elevated field was intended to nullify any effects of magnetic hardness.

Owing to the problem of eddy-current heating in the sample whose area normal to the beam and the field is 3.6 cm^2, a support essentially free of transmitted vibration was required. This need is enhanced by the four mechanical vacuum pumps in the gas handling apparatus associated with the dilution refrigerator and the large Rootes blower system using two motors totaling 30 hp associated with the LMN system. Accordingly, a 2300-kg slab of marble supported by three pneumatic pistons mounted on three 27-cm-diam × 2.5-m-high aluminum pillars was used as a foundation from which the cryostat was suspended. With this support, the minimum temperature attainable was essentially independent of surrounding machinery for applied magnetic fields up to 15 kOe.

Of major concern in cooling any sample external to the mixing chamber is the problem of thermal conductivity at these reduced temperatures. Although the refrigerator may be capable of a given cooling rate, there may exist a considerable thermal gradient between the actual target and the mixing chamber. Considerable effort was expended in minimizing the sources of poor thermal conductivity. The rod connecting the target holder to the mixing chamber was composed of 99.999% pure copper and was annealed in a hydrogen atmosphere after machining. Both the connection to the mixing chamber and to the target holder were threaded connections clamped by a nylon ring whose coefficient of thermal expansion is large compared to the metal threaded parts. Although the thermal conductivity of these threaded joints was measured directly, indicating a negligible gradient across the joint, the thermal conductivity between the $NpAl_2$ grains and the target holder could not be readily determined. Although a temperature of 135 mK on the outer surface of the mixing chamber was measured throughout the course of this experiment, the observed polarization, ~20%, indicated an actual temperature of the $NpAl_2$ considerably higher, ~650 mK. In contrast, a sample in thermal equilibrium with the mixing chamber at 135 mK would be expected to have a polarization of 76%. It is assumed that poor thermal conductivity between the $NpAl_2$ grains and the aluminum matrix, and between the aluminum matrix and the aluminum target holder, would account for the high temperature gradient inferred.

Originally, concern regarding depolarization dictated the choice of polarization axis with respect to the beam direction. If it is desired to have both the beam and target polarized in a direction perpendicular to the neutron flight direction, then passage of the beam through the gap of a superconducting split coil is required. Computer calculations demonstrated that for a neutron beam of 3.6-cm^2 cross-sectional area and a split coil of realistic size, considerable depolarization resulted for neutrons passing through regions of field reversal off the mid plane between the two coils. Hence, the decision was made to polarize the beam and target along the axis of the beam. The neutron beam then passes through the bore of the coils with no resultant depolarization. For s-wave neutrons, there is no distinction between these two configurations. Even for p-wave neutrons, essentially the same quantity of information regarding the total angular momentum of a compound nuclear state formed is retained.

In attempting to determine the cause of the reduced observed polarization, the possibility of depolarization of the neutron beam in the region

between the LMN crystal and the ^{237}Np target was examined. It was ultimately concluded that any depolarization effects were negligible.

C. Neutron Detection Apparatus

Previously, the few experiments that have been conducted with both a polarized neutron beam and target involved measuring the total cross section by observing the transmitted neutrons. Recently, a series of experiments[17,18] have been performed using an unpolarized neutron beam with aligned targets of fissionable nuclei, where the angular distribution of the fission fragments was measured by detecting the fission fragments themselves. In the experiment reported here, the fission neutrons were observed. This permitted use of a thick sample, large solid angle for detected radiation, and detectors external to the cryogenic apparatus. However, the problem of background was introduced since the neutron detectors used are sensitive to γ radiation.

The fission neutron detectors used were liquid-organic scintillators, PSD2, manufactured by Pilot Chemical Corporation, in the form of right cylinders of dimension 12.5 cm × 12.5 cm, mounted on RCA 4525 photomultiplier tubes. In all, 12 detectors were used, subtending a total solid angle of about one π sr. Four of the detectors were positioned at 10° with respect to the beam and the remainder at 90°. Each photomultiplier tube was positioned inside a high-permeability magnetic shield, and was further shielded by a soft iron tube which formed the core of a lead shield around both the scintillator and photomultiplier tube. The lead was necessary to shield the detector from the low-energy γ radiation resulting from the natural decay of ^{237}Np.

Pulse-shape discrimination (PSD) techniques, whereby a scintillation caused by a γ ray and a neutron are distinguished by their different decay times, were used to decrease the sensitivity of the detection system to γ rays. The PSD method selected for this experiment is the simple one of measuring the rise time of the integrated light from the scintillator.[19]

The timing information is determined with crossover pickoff units. The signals from these units are transmitted ~100 m to the data acquisition system, where they are regenerated by discriminators. The symmetric signal starts a time-to-amplitude converter (TAC), while the asymmetric signal provides the stop signal. The TAC contains a single-channel analyzer (SCA) which generates an output pulse for times within a preset window or a second output for times greater than the upper level of the window. These two pulses are fed to a routing network which identifies the detector group and particle type (neutron or γ ray) for the acquisition system. The timing information and particle identification signals from each group of detectors, as well as the timing signal from the transmission detector, are brought together in a routing and gating network which performs several functions. This network provides the stop signal to the clock, which digitizes the time of flight of the neutron and also provides the routing information bits to the clock, identifying each stop signal according to detector group and particle type. The number of γ-ray events are prescaled by a factor of 100 to prevent overloading of the data acquisition computer. Multiple events, which would introduce routing errors, are rejected. The neutron and γ-ray information from each detector group, along with the transmitted neutron information, are then stored in 10 000-channel segments on a fast, random-access disc memory attached to an SEL810-B computer.

The ORELA was used as a pulsed source of neutrons. The operating conditions and other parameters pertinent to this experiment are given in Table II.

III. EXPERIMENTAL RESULTS

The relative fission cross section from 1–1000 eV has been measured by detecting fission neutrons at 10 and 90° relative to the incident beam. In addition, the transmission has been measured from 1–102 eV. The data are composed of four pairs of runs, each run of approximately 24 h duration. Each pair is composed of one 24-h run with the beam and target polarization parallel, and a run of equal duration but with the beam polarization reversed. Within each pair of runs, all operating parameters were held constant to minimize systematic errors, and the duration of each run was determined by monitoring the actual production of neutrons in the accelerator target

TABLE II. Experimental parameters.

Flight path	13.4 m
Moderator	water
Sample areal density	1.6×10^{-3} atoms/b
Neutron burst width	30 nsec
Repetition rate	1000 pps
Average electron-beam power on target	50 kW
Variable channel width	4–512 nsec
Filters	Pb (12.7 mm) Cd (0.64 mm) ^{10}B (0.047 g/cm^2)

room. The useful energy range of the fission data was determined by the signal-to-background ratio; whereas the transmission data were limited entirely by resolution since, in the latter case, the pertinent spacing is D_I, the spacing of "class I" states.

Processing of the data was performed on a CDC-6600 computer. This involved dead-time correction, correcting for variable channel widths, conversion from time of flight to energy, background subtraction, and summing groups within a single run. Processing of runs in a particular pair was performed identically. For example, an average background was subtracted from each run, rather than a separate one for each run. The processed data were then integrated over each resonance and the ratio of these integrals determined for the parallel and antiparallel cases, resulting in four independent determinations of the total angular momentum, J, for each resonance.

The transmission of a polarized neutron beam through a polarized target is given by[6]

$$T = e^{-N\sigma_0}(\cosh f_I f_N N\sigma_0 \mp f_n \sinh f_I f_N N\sigma_0), \quad (5)$$

where N is the target thickness in atoms/cm^2, σ_0 is the cross section in the absence of polarization, f_N is the polarization of the target, f_n is the polarization of the neutron beam, and f_I is a spin-dependent factor given by

$$f_I = \frac{I}{I+1} \quad \text{for } J = I + \tfrac{1}{2},$$

$$f_I = -1 \quad \text{for } J = I - \tfrac{1}{2}.$$

The choice of a $-$ or a $+$ sign in Eq. (5) is determined by whether the polarization of the beam and target are parallel or antiparallel, respectively. In this experiment, the quantities which are determined are the ratios $T_{\text{par}}/T_{\text{anti}}$, for the transmission measurements, and $R_{\text{par}}/R_{\text{anti}}$, where R is the fission reaction rate. It may be shown from Eq. (5) that

$$\frac{T_{\text{par}}}{T_{\text{anti}}} = \frac{1 - f_n \tanh f_I f_N N\sigma_0}{1 + f_n \tanh f_I f_N N\sigma_0} \approx 1 - 2 f_n \tanh f_I f_N N\sigma_0. \quad (6)$$

Similarly, for the fission case

$$\frac{R_{\text{par}}}{R_{\text{anti}}} = \frac{1 - e^{-N\sigma_0}(\cosh f_I f_N N\sigma_0 - f_n \sinh f_I f_N N\sigma_0)}{1 + e^{-N\sigma_0}(\cosh f_I f_N N\sigma_0 + f_n \sinh f_I f_N N\sigma_0)}. \quad (7)$$

Using series expansions of the quantities in Eq. (7) and ignoring all terms of order two or greater in $N\sigma_0$, Eq. (7) reduces to

$$\frac{R_{\text{par}}}{R_{\text{anti}}} = \frac{1 + f_I f_N f_n}{1 - f_I f_N f_n}. \quad (8)$$

For the subthreshold fission resonances measured in this experiment, the difference between Eqs. (7) and (8) is negligible.

The measured ratios for those resonances observed in fission are given in Table III. The quantities $R_\mu = \langle R_{\text{par}}/R_{\text{anti}} \rangle$, are the mean ratios determined from the four independent pairs of runs. The two columns of errors represent the standard deviations from the mean and the statistical errors. The average values of the R_μ for each J value are also indicated in the table. Clearly, the relative J value for each resonance is generally well determined. However, the correct absolute J value assignment requires that the sign of the product μH in Eq. (4) be known; that is, that the direction of target polarization relative to the impressed magnetic field be known. Evidence from three separate observations to be discussed in detail below indicates that the sign of μH is

TABLE III. Fission measurements. Weighted mean $R\mu$: $J=2$, $\langle R_\mu \rangle = 0.79 \pm 0.04$; $J=3$, $\langle R_\mu \rangle = 1.17 \pm 0.02$.

E_0	$R_\mu = \left\langle \frac{R_{\text{par}}}{R_{\text{anti}}} \right\rangle$	σ_μ	Statistical error	J
26.6	1.259	±0.060	0.131	3
30.4	1.086	0.074	0.042	3
37.1	1.163	0.064	0.060	3
38.9	1.091	0.031	0.034	3
39.2	1.134	0.036	0.047	3
39.9	1.169	0.023	0.017	3
41.3	1.201	0.041	0.036	3
46.0	1.160	0.035	0.066	3
50.4	1.409	0.084	0.154	3
119	1.207	0.046	0.042	3
188	0.467	0.153	0.243	2
195	0.818	0.080	0.079	2
201	1.160	0.036	0.035	3
207	1.393	0.176	0.292	3
229	0.721	0.218	0.150	2
234	0.839	0.133	0.080	2
253	1.316	0.091	0.098	3
283	0.946	0.140	0.073	(2)
370	0.804	0.143	0.119	2
373	0.745	0.151	0.084	2
427	1.514	0.284	0.158	3
476	0.819	0.160	0.132	2
668	1.459	0.616	0.437	3
718	1.918	0.409	0.449	3
808	1.984	0.306	0.240	3
873	0.810	0.209	0.116	2
884	1.182	0.078	0.146	3

positive and, therefore, that for $R_{par}/R_{anti} > 1$, $J = I + \frac{1}{2} = 3$.

Perhaps the strongest evidence arises from Eq. (8). For a given product polarization $f_n f_N$, the ratio R for a resonance of $J = I + \frac{1}{2}$ differs from one of $J = I - \frac{1}{2}$ due to different values of f_I. For ^{237}Np, the two f_I values are $\frac{5}{7}$ and -1. The ratios given in Table III are labeled assuming μH to be positive. Using the deduced value of neutron beam polarization of $f_n = 0.55$ and the average values of R_μ and solving Eq. (8) for the target polarization f_N, one determines $f_N = 0.20$ from the $J = 3$ ratios and $f_N = 0.21$ from the $J = 2$ ratios. If, however, one assumes that μH is a negative quantity, then the correct R_μ would be the reciprocals of the values in Table III. Again, solving for f_N in Eq. (8), the observed values of f_N become 0.30 for $J = 3$ and 0.14 for $J = 2$. Since the errors on the average ratios R_μ used in this calculation are quite small, clearly only the former assumption of μH positive is tenable.

TABLE IV. J assignments from transmission.

E_0	R_μ	σ_μ	J	E_0	R_μ	σ_μ	J
1.47	0.932	±0.002	2	38.20	1.055	0.011	3
1.96	1.133	0.014	3	38.90	1.024	0.018	3
3.07	1.854	0.864	(3)	39.20	1.061	0.042	3
3.85	1.082	0.005	3	39.90	1.028	0.050	(3)
4.26	0.793	0.015	2	41.30	1.123	0.027	3
4.86	0.874	0.007	2	43.60	0.747	0.087	2
5.76	1.062	0.003	3	45.70	0.827	0.048	2
6.36	1.104	0.023	3	46.00	1.070	0.004	3
6.65	0.820	0.082	2	46.30	1.108	0.018	3
7.18	0.382	0.089	(2)	47.30	0.874	0.007	2
7.42	1.121	0.009	3	48.80	0.967	0.022	2
8.29	1.133	0.015	3	49.80	1.095	0.015	3
8.96	1.114	0.021	3	50.40	1.060	0.005	3
9.28	0.879	0.004	2	52.20	0.669	0.123	2
10.20	0.761	0.107	2	52.60	0.860	0.074	2
10.70	1.081	0.012	3	53.90	0.891	0.078	2
10.80	1.060	0.007	3	55.00	1.326	0.266	3
11.10	0.900	0.008	2	56.10	0.980	0.032	(2)
12.20	1.042	0.100	(3)	58.40	1.375	0.212	3
12.60	0.895	0.011	2	59.50	0.920	0.055	2
13.10	1.148	0.282	(3)	60.00	1.127	0.079	3
15.80	1.213	0.226	(3)	61.00	1.263	0.070	3
16.10	0.890	0.009	2	61.70	1.787	0.370	3
16.80	0.897	0.013	2	62.50	1.107	0.043	3
17.60	1.142	0.047	3	62.90	1.086	0.042	3
18.90	0.901	0.033	2	65.00	1.114	0.147	(3)
19.10	1.390	0.142	3	65.70	1.072	0.028	3
19.90	1.111	0.120	(3)	66.70	1.013	0.007	(3)
20.40	0.892	0.006	2	67.50	1.067	0.017	3
21.10	1.077	0.009	3	68.00	0.928	0.012	2
22.00	0.880	0.012	2	68.70	1.204	0.192	3
22.90	1.045	0.011	3	70.30	1.203	0.061	3
23.70	1.080	0.008	3	71.10	1.082	0.028	3
24.00	0.845	0.017	2	74.40	0.976	0.068	(2)
25.00	1.054	0.012	3	78.40	1.060	0.018	3
26.20	1.092	0.048	3	79.20	0.842	0.030	2
26.60	1.076	0.014	3	80.70	1.756	0.578	3
28.50	0.694	0.121	2	82.20	1.190	0.154	3
28.90	0.946	0.097	(2)	86.50	1.062	0.009	3
29.50	0.560	0.178	2	87.70	0.885	0.029	2
30.40	1.070	0.012	3	90.90	1.056	0.016	3
31.30	1.285	0.198	3	93.40	0.907	0.052	2
33.40	1.084	0.078	3	97.90	0.948	0.015	2
33.90	0.787	0.049	2	98.60	0.821	0.053	2
34.70	1.325	0.227	3	100.30	1.061	0.008	3
35.20	0.894	0.048	2	101.10	0.920	0.035	2
36.40	1.302	0.250	3				
37.10	1.097	0.013	3				

As supporting evidence, calculations[20] of hyperfine fields in actinide compounds based on systematic interpretation of Mössbauer data indicate that for a hyperfine field of the magnitude of that observed in $NpAl_2$, the sign must be positive.

Additional evidence from the measurements described here is based upon the assumption that the level density observed where no nonstatistical mechanism, such as the intermediate structure in the fission channel, is expected to be present, should vary according to $2J+1$. In Table IV, the resonances observed in transmission are listed with their spin assignments. The mean measured ratios of the areas under each resonance for polarizations parallel and antiparallel are also given, as for the fission resonances in Table III, along with the standard deviation from the mean. Assignments are put in parentheses whenever the error is large compared to the deviation from unity or if the resonance is particularly small. Of these resonances, 57 are assigned $J = 3$ and 37 $J = 2$. Although the statistical error is large on this sampling, the $2J+1$ dependence is sup-

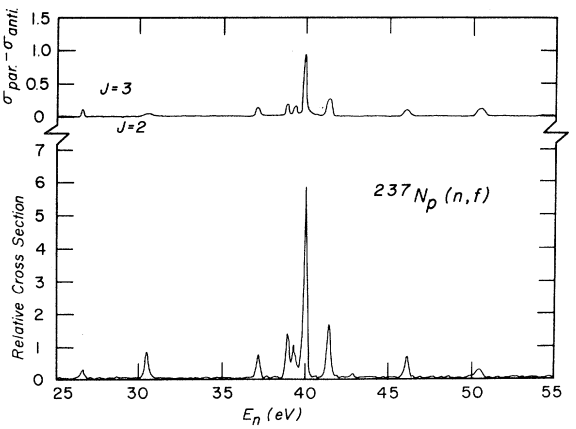

FIG. 5. The fission data in the region of the first intermediate structure group at 40 eV. The upper curve represents the difference between the data for the configuration of beam and target polarization parallel and antiparallel. This curve remains positive over each resonance, indicating $J = 3$ for each resonance.

ported with these assignments and strongly violated for the opposite spin assignments.

The fission data in the region of the 40-eV structure are shown in Fig. 5. The enhancement of the compound nuclear levels is distributed over nine individual resonances. The curve representing $\sigma_{par} - \sigma_{anti}$ demonstrates that all the individual resonances are of the same spin, $J=3$. A sample of the transmission data is shown in Fig. 6, over the range 4–18 eV. Here the plot of $T_{par} - T_{anti}$ demonstrates the clear distinction between resonances of opposite spin.

The fission data shown and tabulated here were derived only from the neutron detectors positioned at 90°. The 10° detectors showed a higher background and, when combined with the 90° data, resulted in a poorer signal-to-noise ratio. However, any possible effects of an anisotropic angular distribution were considered. On the larger resonances, no significant difference between the ratio R_{par}/R_{anti} at 10 and at 90° was observed.

IV. DISCUSSION

The difficulty of spin determination by methods less direct than that employed in this experiment is well known. For example, spin assignments in the system $^{235}U+n$ are in wide disagreement. An experiment on ^{235}U using the equipment and techniques described here will be reported in a subsequent paper. Although far less effort has been expended on ^{237}Np, comparison of J assignments from this experiment and from a measurement[21] of the total, scattering and capture cross sections demonstrates the ambiguity of indirect spin determination. As shown in Table V, the two sets of spin assignments are in only random agreement. Not only do the assignments for these resonances in the 40-eV structure differ,

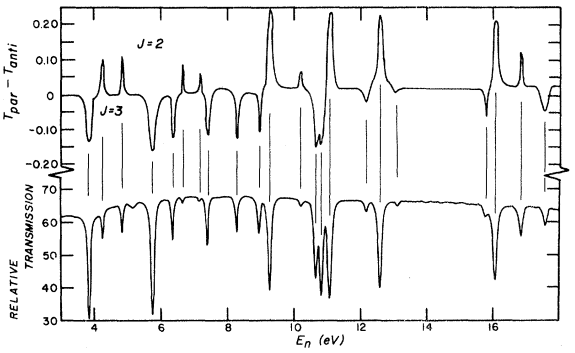

FIG. 6. A sample of the transmission data. The upper curve represents the difference between the transmission for beam and target polarization parallel and antiparallel. The curve dips below zero for resonances with $J=3$ and protrudes above zero for those with $J=2$.

TABLE V. Comparison of J assignments.

E_0	Present work J	Poortmans *et al.* (Ref. 21) J
5.76	3	3
10.8	3	3
11.1	2	2
12.6	2	3
16.1	2	2
20.4	2	3
22.0	2	3
23.7	3	3
25.0	3	2
26.6	3	2
30.4	3	2
46.3	3	(3)
47.3	2	(3)
50.4	3	3

but those for the resonances below 26 eV are in agreement in only four out of nine cases.

Reference 21 also indicates a possible spin dependence of the mean capture width, $\langle\Gamma_\gamma\rangle = 47$ meV for $J=3$ resonances and 57 meV for those with $J=2$. However, as Table VI indicates, when the present spin assignments are applied to the capture widths of Ref. 21, the mean width is the same for both spin states. Similarly, examining a total of 62 resonances whose reduced neutron widths are compiled in Ref. 22 and whose spins are determined here, no dependence on spin is observed, within the sizeable errors. The average values, $\langle\Gamma_n^0\rangle$, are also given in Table VI.

However, a detailed comparison of the present results with the observations of Kuiken, Pattenden, and Postma[18] is somewhat enlightening, although complex. In that experiment, an aligned target and unpolarized neutron beam were used to obtain information about the K quantum number, the projection of J on the nuclear symmetry axis. The angular distribution of the fragments themselves were measured. This angular distribution is expressed by an expansion in terms of even Legendre polynomials:

$$W(\theta) = 1 + \sum_{m=2,4\ldots} A_m f_m P_m(\cos\theta), \tag{9}$$

TABLE VI. J dependence average widths.

$J=2$	$J=3$
$\langle\Gamma_\gamma\rangle = 51.7 \pm 3.2$ meV	$\langle\Gamma_\gamma\rangle = 52.3 \pm 1.7$ meV
$\langle\Gamma_n^0\rangle = 0.019 \pm 0.007$ meV	$\langle\Gamma_n^0\rangle = 0.018 \pm 0.006$ meV

where the f_m are the orientation parameters (e.g., $f_2 \equiv$ alignment). The parameters A_m depend on the quantum numbers of the transition states. For the experimental conditions realized in the experiment of Ref. 18, the f_4 parameter is negligible compared to f_2, and the quantity of interest becomes A_2, given explicitly by

$$A_2 = \frac{15}{4}\frac{I}{I+1}\left(\frac{3K^2}{J(J+1)} - 1\right) . \quad (10)$$

Without knowledge of the J value of a resonance, it becomes quite difficult to determine unique K values. This difficulty is further enhanced by uncertainty as to whether the observed K must have only integral values or whether there may exist some admixture from higher transition states.

The nature of the deformation barriers and the possible effects upon the observed K values is discussed in Ref. 18. Current evidence in the form of a broad low peak under the 40-eV structure, observed by Paya *et al.*,[4,5] and the lack of lines in the γ-ray spectrum corresponding to transitions between intermediate levels in the second well, indicate very weak coupling between the compound nuclear levels and the intermediate levels. This corresponds to a situation where the second barrier, at higher deformation, is lower than the first barrier. In this case, there may be some admixing of higher transition states, although Kuiken, Pattenden, and Postma assume that this admixing is small.

TABLE VII. J vs A_2 parameters. Theoretical A_2 values:

$(J:K)$	A_2	$(J:K)$	A_2
(2:0)	−2.679	(3:0)	−2.679
(2:1)	−1.339	(3:1)	−2.009
(2:2)	+2.679	(3:2)	0
		(3:3)	+3.348

Mean observed A_2 values: $J=2$: $\langle A_2\rangle = 1.38 \pm 0.35$; $J=3$: $\langle A_2\rangle = 2.42 \pm 0.24$; 40-eV group $\langle A_2\rangle = 2.56 \pm 0.24$; other groups $\langle A_2\rangle = 0.76 \pm 0.50$.

E_0	J	$A_{2[15]}$
26.6	3	2.98 ± 1.21
30.4	3	3.50 ± 0.47
37.1	3	0.62 ± 0.97
38.9	3	1.82 ± 0.45 [a]
39.2	3	
39.9	3	2.73 ± 0.26
41.3	3	2.36 ± 0.46
46.0	3	1.57 ± 1.00
50.7	3	3.25 ± 1.06
119	3	2.56 ± 0.21
193	2	−0.13 ± 0.57 [a]
203	3	
231	2	1.84 ± 1.45
253	3	−0.02 ± 1.30
283	(2)	0.57 ± 1.72
371	2	1.47 ± 1.34
427	3	−0.37 ± 1.87
873	2	1.86 ± 1.74 [a]
884	3	

[a] Unresolved in Ref. 18.

In Table VII, a composite list of individual resonances, including spin assignments and the A_2 values determined in Ref. 18, is given, along with the theoretical A_2 values from Eq. (10). Poor resolution averages several of the A_2 values over more than a single resonance or structure. Assuming an assignment of $J=2$ for the 40-eV structure, Kuiken, Pattenden, and Postma concluded that the evidence was consistent with an integral K value, $K=2$, for the individual resonances in that group. However, the present assignment of $J=3$ to this group makes this interpretation less consistent with an integral K value and implies an admixture of $K=3$ and $K=2$ components. In most cases, the $K=3$ component seems predominant, although insufficient to explain many of the A_2 values. Interpretation of the alignment data becomes more ambiguous at higher energies, owing to larger statistical errors, although the same basic conclusion seems to apply. The structure at 119 eV has a measured A_2 value in between the expected for a resonance with $(J:K)=(3:3)$ and for one with (3:2). Similarly, the three structures at 231, 283, and 370 eV, all of which are assigned $J=2$, are most consistent with a mixture of $K=2$ and $K=1$ components. The pairs of structures near 200 and 870 eV were unresolved in the alignment data and, since the members of those pairs are of opposite spin, are difficult to interpret. The remaining structures appear to be consistent with integral K assignments of $(J:K)=(3:2)$.

Some conclusions may be drawn from the mean A_2 values for each spin state shown in Table VII. In both cases, it appears that the $K=0$ transition states are unavailable. This implies that the unpaired neutron and proton in ^{238}Np couple to higher spin states. The observed $\langle A_2\rangle$ values can be explained by noting that the $K=2$ channel is generally preferred with $(J:K)=(2:1)$ and (3:3) partially open. The mean A_2 value for the $J=3$ resonances would imply that the $K=3$ channel is preferred, but this is primarily a result of the small errors on those resonances in the 40-eV structure. Those resonances in the 40-eV clump appear to preferentially decay through $K=3$ transition states, whereas the remaining $J=3$ structures prefer $K=2$ channels.

V. CONCLUSIONS

From the experimental results described here, several conclusions may be drawn. The Strutinsky theory of a double-humped fission barrier is substantiated as the mechanism by which intermediate structure in subthreshold fission is explained. The coupling of the "class II" states in the second well to the compound nuclear levels in the first well selects resonances of a single-spin state, that of the "class II" state. From examination of existing data[18] on the angular distribution of fission fragments from aligned ^{237}Np with the spin assignments reported here, one observes that, at least in the odd-odd system ^{237}Np$+n$, there is an admixing of transition states, evidenced by nonintegral values of the projection quantum number, K. Although all values of K from zero to J are allowed, the value $K=2$ appears to be predominant for both $J=2$ and 3, with contributions from $K=3$, $J=3$, and $K=1$, $J=2$ states. The specific nature of the excitations in the second well is difficult to predict, since there is both an odd proton and odd neutron. It is known that the ground state of ^{238}Np at equilibrium deformation is a 2^+ level, although the spin and parity of the ground state at the larger deformation of the second barrier could be different.

In contrast to the fission results, the total cross section shows no intermediate structure but rather a $2J+1$ distribution of resonances. Similarly, no nonstatistical spin dependence is observed in the capture or neutron widths.

ACKNOWLEDGMENTS

The authors wish to express their gratitude to Dr. M. S. Moore for his suggestions and continual interest in this project during its duration of several years, and to Dr. B. C. Diven for his support and advice during that time. In addition, the efforts of J. M. Anaya and J. J. Bautista in preparing and operating the equipment is highly appreciated. We are also indebted to the staff of the Oak Ridge electron linear accelerator and to Dr. J. D. Rogers and Dr. J. R. Bartlit of the Los Alamos Scientific Laboratory cryogenics group. Finally, the assistance of Dr. W. A. Steyert, Dr. J. C. Wheatley, and Dr. W. C. Black in questions of low temperature phenomena was invaluable.

---

†Work performed under the auspices of the U. S. Atomic Energy Commission.

*Present address: International Atomic Energy Agency, Vienna, Austria.

[1]V. M. Strutinsky, Nucl. Phys. A95, 420 (1967).

[2]J. E. Lynn, United Kingdom Atomic Energy Research Establishment Report No. AERE-R 5891, 1968 (unpublished); in *Proceedings of the Symposium on Physics and Chemistry of Fission* (IAEA, Vienna, 1969), p. 249.

[3]H. Weigman, Z. Phys. 214, 7 (1968).

[4]D. Paya, H. Derrien, A. Fubini, A. Michaudon, and P. Ribon, *Nuclear Data for Reactors* (IAEA, Vienna, 1968), Vol. II, p. 128.

[5]D. Paya, J. Blons, H. Derrien, and A. Michaudon, in *Proceedings of the Symposium on Physics and Chemistry of Fission* (IAEA, Vienna, 1969), p. 307.

[6]A. Stolovy, Phys. Rev. 118, 211 (1960); 134, B 68 (1964).

[7]H. Postma, H. Marshak, V. L. Sailor, F. J. Shore, and C. A. Reynolds, Phys. Rev. 125, 979 (1962).

[8]F. L. Shapiro, *Nuclear Structure Study with Neutrons* (North-Holland, Amsterdam, 1966), p. 223.

[9]C. D. Jeffries, *Dynamic Nuclear Orientation* (Interscience, New York, 1963).

[10]A. Abragam and M. Borghini, *Progress in Low Temperature Physics* (North-Holland, Amsterdam, 1964), Vol. 4, p. 384.

[11]P. Draghicescu, V. I. Lushchikov, V. G. Nikolenko, Yu. V. Taran, and F. L. Shapiro, Phys. Lett. 12, 334 (1964).

[12]C. J. Gorter, Physica 14, 504 (1948).

[13]M. E. Rose, Phys. Rev. 75, 213 (1949).

[14]B. D. Dunlap, M. B. Brodsky, G. M. Kalvius, G. K. Shenoy, and D. J. Lam, J. Appl. Phys. 40, 1495 (1969).

[15]Superconductivity Helium Electronics Manufacturing Corporation, 3422 Tripp Court, Suite B, San Diego, California 92121.

[16]J. R. Sites, H. A. Smith, and W. A. Steyert, J. Low Temp. Phys. 4, 605 (1971).

[17]N. J. Pattenden and H. Postma, Nucl. Phys. A167, 225 (1971).

[18]R. Kuiken, N. J. Pattenden, and H. Postma, Nucl. Phys. A196, 389 (1972).

[19]F. T. Kuchnir and F. J. Lynch, IEEE Trans. Nucl. Sci. NS-15, No. 3, 107–113 (1968).

[20]B. D. Dunlap and G. M. Kalvius, Int. J. Magn. 2, 231 (1972).

[21]F. Poortmans, H. Ceulemans, J. Theobald, and E. Migneco, in *Proceedings of the Third Conference on Neutron Cross Sections and Technology, Knoxville, 1971*, AEC Report No. CONF-710301 (U.S. GPO, Washington, D.C., 1971), Vol. 2, p. 667.

[22]*Neutron Cross Sections*, compiled by J. R. Stehn, M. D. Goldberg, R. Wiener-Chasman, S. F. Mughabghab, B. A. Magurno, and V. M. May, Brookhaven National Laboratory Report No. BNL-325 (U.S. GPO, Washington, D. C., 1965), 2nd ed., 2nd Suppl., Vol. III, Z=88–98.